










ACCEPTED MANUSCRIPT

Alberto Strini<sup>1,\*</sup>, Alessandra Sanson<sup>2</sup>, Elisa Mercadelli<sup>2</sup>, Riccardo Bendoni<sup>2,3</sup>, Marcello Marelli<sup>4</sup>, Vladimiro Dal Santo<sup>4</sup> and Luca Schiavi<sup>1</sup>

**In-situ anatase phase stabilization of titania photocatalyst by sintering in presence of Zr<sup>4+</sup> organic salts**

*Applied Surface Science* 347 (2015) 883–890

doi: [10.1016/j.apsusc.2015.04.155](https://doi.org/10.1016/j.apsusc.2015.04.155)

<sup>1</sup> Istituto per le Tecnologie della Costruzione (ITC-CNR), via Lombardia, 49 – I-20098 San Giuliano Milanese (MI) – Italy

<sup>2</sup> Istituto di Scienza e Tecnologia dei Materiali Ceramici (ISTEC-CNR), via Granarolo, 64 – I-48018 Faenza (RA) – Italy

<sup>3</sup> Dipartimento di Scienze e Tecnologie Chimiche e Centro NAST - Università di Roma Tor Vergata, via della Ricerca Scientifica – I-00133 Roma – Italy

<sup>4</sup> CNR – Istituto di Scienze e Tecnologie Molecolari, via Golgi, 19 – I-20133 Milano – Italy

**Abstract**

The direct in-situ stabilization of an anatase-based nanocrystalline photocatalyst (Degussa P25) was obtained by sintering the catalyst powder in presence of Zr<sup>4+</sup> organic salts. This approach allows the doping of an already-formed nanocrystalline photocatalyst instead of introducing the dopant in the crystal lattice during the catalyst synthesis. The procedure was demonstrated by the production of thick ceramic layers using the screen printing technique. This new method allows to easily stabilize the anatase phase 200 °C higher than the undoped P25 maintaining the same photocatalytic activity. The process was studied using specifically formulated screen-printing inks added with Zr<sup>4+</sup> organic salt at 1% and 2% Zr/Ti molar ratio. The anatase phase stability was investigated in the 500–900 °C temperature range analysing the resulting catalysts with XRD, TEM and (S)TEM-EDS. The catalytic activity of the screen-printed layers was assessed by measuring the degradation of toluene in air at ambient concentration (500 nmol m<sup>-3</sup>) and low UV-A irradiance (180 μW cm<sup>-2</sup>). The described in-situ stabilization method could be potentially applied to any deposition process involving already formed anatase photocatalyst, allowing higher sintering temperature and then an improved mechanical stability of the active layers without photocatalytic activity degradation.

**Keywords**

anatase to rutile conversion; anatase stabilization; zirconium doped titanium dioxide; screen-printed photocatalyst layer; gas-solid photocatalysis

## 1. Introduction

Titanium dioxide, particularly in nanocrystalline form, is of great interest for several applications, including photocatalysis for air/water depollution, solar cells and hydrogen production by water splitting. The use of the anatase or mixed anatase/rutile crystalline phase is generally considered preferable to the less reactive rutile phase [1]. The anatase phase however, while typically kinetically favoured in several catalyst synthesis processes, is metastable and transforms into the thermodynamically stable rutile at temperatures higher than 500 °C [2, 3]. This is a particularly undesirable limitation in several deposition technologies, where high temperature processing is required for sintering and mechanically stabilizing the deposited layers. The improvement of the anatase thermal stability has therefore become an important field of study. The most common strategy involves the direct synthesis of anatase nanocrystals doped with transition metals or rare earths, such as zirconium [4–7], lanthanum [8–10], cerium [11], europium and samarium [12]. The use of fluoride [13], sulphur [14] and nitrogen [15] as dopant was also reported.

However, all these works are focused only on the ex-novo syntheses of thermally stable doped-anatase: to the author's knowledge post-synthesis stabilization of already formed anatase nanocrystals has never been addressed. The latter is potentially of great interest because it can pave the way to the use of commercially available anatase-based photocatalysts in high temperature ceramic processes, such as screen-printing technology.

The present work describes the stabilization of the anatase phase of a commercially available titania photocatalyst (Degussa P25) by a novel process based on sintering in presence of  $Zr^{4+}$  organic salts, demonstrating an increase of up to 200 °C in the phase transition temperature and a high photocatalytic activity of the resulting titania layers even after a thermal treatment at 800 °C.

The procedure was integrated in the screen-printing deposition process combining the  $Zr^{4+}$  organic salt and the photocatalyst into a specifically developed screen printing ink formulation, resulting in a rapid and effective stabilization method for the production of photocatalyst layers.

Finally, the photocatalytic activity of the obtained layers was assessed by measuring the toluene degradation in air at ambient concentration and low irradiance.

## 2. Experimental

All air concentrations, volumetric flows and R.H. values in this work are given at 25 °C, 101.3 kPa reference conditions.

### 2.1. Sample preparation

All screen-printed and powder samples were prepared at ISTECC-CNR laboratories using a single batch of  $TiO_2$  (Degussa P25) with 80/20 anatase/rutile phase ratio (Section 3.1) and, according to the supplier,  $50 \pm 15 \text{ m}^2 \text{ g}^{-1}$  specific surface area (Brunauer-Emmett-Teller) with 21 nm average particle size. The screen-printed samples were prepared as previously described [16] using specially formulated inks according to the different content of  $Zr^{4+}$ . All the inks were optimized in order to obtain  $0.75 \text{ mg cm}^{-2}$  titania loading (area-specific mass) on the final screen-printed films. The inks were prepared using terpeneol (isomer mixture, Aldrich) as solvent and adding the  $TiO_2$  powder and the proper amount of lauric acid ( $\geq 99.5\%$ , Aldrich) and ethyl cellulose (Fluka) used as deflocculant and binder, respectively. The  $Zr(IV)$  2,4-pentanedionate (Alfa Aesar) was pre-dissolved in terpeneol and directly added to the suspension in the required amounts (Table 1). After a preliminary manual mixing, each prepared ink suspension was ball-milled for 24 h and then fine milled with a three-roll

grinding mill equipped with zirconia rollers of nanometric finishing (Exakt 80E, Exakt, Nordestedt, Germany) to improve homogeneity as previously reported [17].

All the layers were printed on commercial 96% alumina substrate (0.62 mm thickness, Aurel Automation S.p.A., Italy). The substrates were prepared in  $26 \times 76$  mm pieces, washed with a NaOH saturated ethanol solution, HCl 1M aqueous solution and finally sonicated in ethanol for 15 min (Transsonic T460H Bath, Elma) to remove organic and inorganic impurities [18]. A suitable mask (165 mesh polyester printing screen) was used to print a  $3 \text{ cm}^2$  ( $15 \times 20$  mm) catalyst area onto the substrates. Thick films were deposited (squeegee speed  $90 \text{ mm s}^{-1}$ , squeegee load 64 N, snap-off distance 0.7 mm) on the pre-cleaned substrate by a single print step using a semiautomatic precision screen printer (Aurel 900, Aurel Automation S.p.A., Italy).

The as-deposited films were dried at ambient conditions and thermally treated according to the conditions reported for each sample in Table 2 with a heating rate of  $100 \text{ }^\circ\text{C h}^{-1}$ . The total amount of catalyst deposited on each sample was determined by weighing the sample substrate before the printing process and after the thermal treatment as previously described [16].

The complete list of all screen-printed samples used in this work is reported in Table 2.

A series of unsupported catalytic powders was prepared from the printing inks in order to study the anatase phase fraction and the powder morphology. These samples were prepared by thermally treating the inks at the same conditions as the corresponding screen-printed samples. The powder sample series includes a high zirconium content sample (7.5% Zr/Ti molar ratio) specially prepared for TEM and XRD analysis.

## 2.2. X-ray diffraction

The powder samples phase composition was studied by X-ray diffraction (D8 Advance with Linxeye detector, Bruker AXS, Germany) using Cu  $K\alpha$  radiation in the  $10\text{--}80^\circ$  ( $2\theta$ ) range, scan by  $0.02^\circ$  steps (92.5 s integration time per step). The quantitative phase analysis was performed following the Reference Intensity Ratio (RIR) technique, while the average crystallite size of the powders was estimated by the XRD patterns, using the Debye-Scherrer equation. The calculation of the cell parameters was performed using the GSAS EXPGUI software following RIR-Rietveld refinement techniques [19, 20].

## 2.3. Specific surface area measurement

The specific surface area (SSA) of selected screen-printed samples was determined at ISTM-CNR laboratories by Kr physisorption at around 77 K, employing a multipoint BET interpolation of adsorption isotherm (ASAP 2020, Micrometitics). Samples were cut in small pieces (about  $0.6 \times 1.7$  cm) using a diamond cutting wheel, paying special attention to not detach the  $\text{TiO}_2$  film. The cut pieces were inserted in a glass ampoule and a filler rod was inserted too, to lower free space. Samples were pretreated at 673 K for 1 h under high vacuum before carrying out Kr adsorption. The molecular area of krypton, saturation pressure at 77 K and other experimental parameters were taken as recommended by the equipment producer. At the end of the pretreatment, all samples were slightly brownish due to the formation of oxygen vacancies and reduced  $\text{Ti}^{3+}$  sites.

## 2.4. Transmission electron microscopy characterization

A series of micrographs were collected with a Libra 200FE (Zeiss) energy-filtering transmission electron microscope (EFTEM) at ISTM-CNR laboratories in order to consolidate the XRD data and to exclude the presence of zirconium oxide nanostructure. All the powder specimens were gently grounded in an agate mortar, suspended in isopropanol and sonicated 15 minutes. A drop of each

suspension was then applied onto a holey carbon coated copper grid and dried overnight. Energy-dispersive X-ray spectroscopy (EDS – Oxford INCA Energy TEM 200) analysis and maps were coupled with high angular annular dark field scanning electron microscopy (HAADF-STEM) micrographs.

### 2.5. Photocatalytic activity measurement

The photocatalytic activity measurements were carried out at ITC-CNR laboratories using a previously described dedicated experimental system [21] based on a continuous-flow stirred photoreactor. The experimental apparatus comprises an artificial air generator, a 2 L photochemical reactor placed into an irradiation chamber and a gas chromatograph with photoionization detector for the measurement of the toluene concentration in the reactor effluent. Because of the reactor stirring, the pollutant concentration in the effluent air stream is representative of the whole reactor internal atmosphere allowing the direct computation of the reaction rate (Section 3.4).

For all measurements, toluene at ambient concentration was considered as model pollutant. The photoreactor supply air was obtained by mixing and humidifying gas-chromatographic grade nitrogen and oxygen (Alphagaz 1, Air Liquide, Italy) with a 500 ppb toluene standard diluted cylinder (SIAD, Italy) using a computer controlled artificial air generator [21]. A 100 mL min<sup>-1</sup> total air supply flow (20.9% O<sub>2</sub> v/v) at 25 ± 0.2 °C, 50 ± 2% R.H. ambient conditions was used for all the measurements. The nominal operating toluene concentration was 500 nmol m<sup>-3</sup> (12.2 ppb) with 500 ± 30 nmol m<sup>-3</sup> actual obtained value for all experiments. The actual value of the toluene concentration inside the photochemical reactor was reached for each measurement by a two-step successive approximation method [16] by varying the flow from the standard toluene cylinder. The total air inlet flow was kept constant by compensation with the pure nitrogen flow. This approach was preferred instead of the operation with constant inlet concentration because the latter causes the internal reactor concentration to vary according to the catalytic activity of each sample, resulting in non-uniform measurement conditions across the whole study [21]. The reactor was operated with 1800 rpm mixing fan speed for all photocatalytic activity measurements. The velocity of the recirculating air inside the reactor, measured at a 27 mm distance from the sample surface as previously described [16], was 0.67 ± 0.05 m s<sup>-1</sup>.

The UV-A source was provided by two fluorescent lamps (PL-S/BLB, Philips). The resulting irradiance at the sample surface, integrated in the 340–400 nm spectral band [21], was 182 ± 5 μW cm<sup>-2</sup> for all photocatalytic activity measurements.

The components of the experimental system (synthetic air generator, irradiation chamber on-line radiometer and thermometer, gas chromatographic analyzer) were calibrated as previously described [21].

All samples were measured without any pre-treatment.

## 3. Results

### 3.1. XRD characterization

The anatase amounts calculated from the XRD spectra of the powder samples sintered at different temperatures and for different times were reported in Fig. 1 and Fig. 2, respectively.

The measured anatase fraction of the as-received P25 is 80 ± 4%. In the pure P25 samples thermally treated for 30 min at different temperatures the decrease of the anatase amount due to its conversion to the rutile phase starts at 600 °C (76 ± 4% residual anatase fraction), is substantial at 700 °C

( $52 \pm 3\%$ ) and is nearly complete at  $800\text{ }^\circ\text{C}$  ( $3.0 \pm 0.1\%$ ). The samples treated at  $900\text{ }^\circ\text{C}$  and  $1100\text{ }^\circ\text{C}$  do not show any measurable residual anatase. The samples with 1% Zr/Ti molar ratio show a substantial stabilization demonstrating  $78 \pm 4\%$  anatase fraction after the thermal treatment at  $700\text{ }^\circ\text{C}$  for 30 min and  $67 \pm 3\%$  after  $800\text{ }^\circ\text{C}$  treatment, the latter being comparable to those measured for the pure P25 treated at  $600\text{ }^\circ\text{C}$ . On the other hand, anatase fraction measured for the samples with 2% Zr/Ti demonstrate an even higher stabilization, with  $29 \pm 1\%$  residual anatase fraction after 30 min at  $900\text{ }^\circ\text{C}$ . The 2% Zr/Ti sample treated at  $800\text{ }^\circ\text{C}$  shows the same anatase fraction as the undoped sample treated at  $600\text{ }^\circ\text{C}$ . The anatase fraction measured for the samples treated at  $700\text{ }^\circ\text{C}$  for different sintering times is reported in Fig. 2. The conversion trend during the thermal treatment is evident for the pure P25 with the anatase fraction dropping to  $35 \pm 2\%$  after 60 min and to  $21 \pm 2\%$  after 180 min. On the other hand, the samples doped with  $\text{Zr}^{4+}$  demonstrate an effective stabilization of the anatase phase, showing only a slight decrease from the 30 min to the 90 min-samples and no further detectable conversion after this time. No formation of crystalline zirconia was detected from XRD data.

The mean anatase crystallite size calculated from the XRD spectra of the powder samples thermally treated at different temperatures for 30 min was reported in Fig. 3. The mean crystallite size of the pure P25 sample treated at  $500\text{ }^\circ\text{C}$  is equal to 23 nm and steadily increases with the rise of the heating temperature reaching 29 nm at  $700\text{ }^\circ\text{C}$  and 43 nm at  $800\text{ }^\circ\text{C}$ . The anatase crystallite size of both 1% and 2% Zr/Ti samples shows a remarkable stability in the 500 to  $800\text{ }^\circ\text{C}$  temperature range. A significant increase of the crystallite size was registered only for the Zr-doped samples thermally treated at  $900\text{ }^\circ\text{C}$ , measuring a mean size of 44 nm and 31 nm for the 1% and 2% Zr/Ti sample respectively (see also Fig. 4).

The cell parameters obtained with the RIR-Rietveld method for the samples treated at  $700\text{ }^\circ\text{C}$  are reported in Table 3 where an increase in cell volume is detectable for samples doped with 1 and 2 mol% of Zr. The same method applied to the 7.5% Zr/Ti molar ratio sample treated at  $700\text{ }^\circ\text{C}$  for 30 min shows a 5.0/95.0 zirconia/titania molar ratio, which indicates that in this sample a considerable amount of the added zirconium (67.4%) is present in form of zirconia phase on the  $\text{TiO}_2$  particle surface while the volume of the lattice is consistent with a doping amount around 2 mol%.

### 3.2. Specific surface area

The SSAs of the catalytic layers treated at  $700\text{ }^\circ\text{C}$  and  $800\text{ }^\circ\text{C}$  were reported in Fig. 5. The data repeatability was evaluated by a triple measurement of the 2% Zr/Ti sample treated at  $800\text{ }^\circ\text{C}$ . All the measured doped samples show higher SSA values than the undoped ones. However, it is worth noting that the 2% Zr/Ti sample sintered at  $700\text{ }^\circ\text{C}$  demonstrates lower SSA than the 1% sample, even though for the  $800\text{ }^\circ\text{C}$  samples the difference falls within the experimental errors. The measurements show also a quite abrupt decrease of the film SSA for the undoped P25 sample after the treatment at  $800\text{ }^\circ\text{C}$  and, to a lesser extent, for the 1% Zr/Ti sample. The SSA for the 2% Zr/Ti sample does not demonstrate a significant variation from the  $700\text{ }^\circ\text{C}$  to the  $800\text{ }^\circ\text{C}$  thermal treatment.

### 3.3. Transmission electron microscopy characterization

The TEM characterization of the low zirconium content samples ( $\text{Zr/Ti} \leq 2\%$ ) shows no evidences of crystalline or amorphous zirconia aggregates. A very different situation was found for the high loaded 7.5% Zr/Ti sample (Fig. 6). The sample shows evident and extensive formation of zirconia aggregates on the titania crystallite surface.

The (S)TEM-EDS mapping images of the 1% and 2% Zr/Ti samples treated at  $700\text{ }^\circ\text{C}$  show a diffuse presence of zirconium, but the small crystallite dimension and the low doping level results in very



noisy signal that does not allow a quantitative determination. However, the images show no evidences of zirconia accumulation as shell structures on the crystal surface or as separated aggregates. A STEM-EDS line analysis was carried out with a >80 nm diameter anatase crystal from the 2% Zr/Ti sample treated at 900 °C for 30 min. The resulting EDS signal profile for zirconium and titanium (independently normalized) were reported in Fig 6. The normalized signal profile for zirconium appears to be closely related to the titanium signal profile, which indicates a uniform dispersion of zirconium in the titania matrix. Particularly, no signs of zirconium signal enhancement near the crystal border were found, which indicates the absence of a significant zirconia shell on the crystal surface. A STEM-EDS map of the same region is also reported in Fig. 7, which confirms the very close correlation between the zirconium and titanium signals. The presence of substantial zirconia deposits found on the anatase crystallite surface of the 7.5% Zr/Ti powder hinders however the search by EDS analysis of Zr<sup>4+</sup> diffusion inside the lattice of titania in this latter sample.

### 3.4. Photocatalytic activity

The photocatalytic reaction rate per surface area (as mass of degraded pollutant per unit of catalytic surface and time) can be directly calculated with the following equation:

$$r = \frac{Q}{A} (C_0 - C) \quad (1)$$

where  $r$  is the reaction rate per surface area ( $\text{mol s}^{-1} \text{m}^{-2}$ ),  $Q$  is the volumetric flow rate ( $\text{m}^3 \text{s}^{-1}$ ),  $A$  is the area of the titania layer surface ( $\text{m}^2$ ),  $C_0$  and  $C$  are the inlet and the reactor internal concentration of the reacting specie ( $\text{mol m}^{-3}$ ), respectively. The reaction rate  $r$  measured at constant toluene concentration for the screen-printed samples sintered at different temperatures for 30 min and at 700 °C for different sintering times are reported in Fig. 8 and in Fig. 9, respectively. The repeatability of the sample photocatalytic activity was measured considering a separate set of five titania screen-printed samples, resulting in  $\pm 9.4\%$  relative standard deviation. The reaction rate data measurement error was calculated as the quadratic sum of the sample activity repeatability and the measurement repeatability (calculated as previously described [16] estimating a  $\pm 2\%$  error in the sample layer surface  $A$ ). The catalytic activity measured for the pure P25 samples thermally treated for 30 min demonstrates a close correlation with the anatase fraction determined for each sample, becoming very low in the sample treated at 800 °C (less than 10% of the activity measured for the samples treated at 500 °C). The 1% Zr/Ti samples demonstrates, after the 800 °C treatment, 80% of the catalytic activity measured after the 500 °C. The activity of the 2% Zr/Ti samples also demonstrates an effective anatase stabilization showing however smaller absolute values with respect to the 1% Zr/Ti samples. The samples sintered at 700 °C for different times show a general activity decrease after longer thermal treatments.

## 4. Discussion

The phase compositions determined by XRD analyses demonstrate a remarkable stabilization of the anatase phase for the Zr<sup>4+</sup> doped P25 powder samples, allowing to increase the sintering temperature by about 200 °C compared to the pure P25. According to the literature, the anatase-rutile phase transition could be inhibited either through the deposition of a thin oxide layer onto the crystalline surface of TiO<sub>2</sub> or by the inclusion of a dopant element inside its crystal lattice. An example of the

first approach is given by lanthanum that retards both the sintering process and the phase transformation by forming a monoatomic layer on the  $\text{TiO}_2$  crystals surface [10]. Such layer is formed because the ionic radius of  $\text{La}^{3+}$  (0.115 nm) is significantly bigger than the one of  $\text{Ti}^{4+}$  (0.068 nm), and therefore its effective insertion into the  $\text{TiO}_2$  lattice is hindered [22]. On the contrary,  $\text{Zr}^{4+}$  is generally considered a dopant for  $\text{TiO}_2$ , since its ionic radius (0.072 nm) allows an effective inclusion in the crystal lattice of the oxide, that could occur through an isomorph substitution or an interstitial insertion. This result was achieved by several authors via *ex-novo* synthesis of anatase in presence of Zr precursors that are thus included in the forming crystal structure [4–7]. It is worth noting that in the present work the doping process was carried out in situ on already formed crystalline materials and not during the catalyst synthesis. The possible inclusion of the  $\text{Zr}^{4+}$  in the  $\text{TiO}_2$  crystals therefore could only involve the solid diffusion of the dopant into the anatase lattice, during the thermal treatment.

The (S)TEM-EDS line analysis and map of zirconium in the 2% Zr/Ti doped sample treated at 900 °C suggests an even distribution of the  $\text{Zr}^{4+}$  in the crystallite, indicating the diffusion of the zirconium in the anatase lattice. This is not surprising considering that this sample underwent a noticeable crystal growth process (as demonstrated by XRD and TEM images) with consequent rearrangement and migration at crystallite level. Despite the low signals, the EDS maps analysis for zirconium and titanium for all the samples with Zr/Ti ratio  $\leq 2\%$  did not show any evidence of zirconia aggregates (that was instead clear for the high  $\text{Zr}^{4+}$  doped ones). All the analyses, TEM imaging, XRD data and (S)TEM-EDS, suggest the presence of a Zr diffusion process. In addition, the high stability of the crystal size demonstrated by the doped samples (that clearly show no crystal growth at treatment temperature  $\leq 800$  °C) is in accordance with other studies in literature involving the doping of  $\text{TiO}_2$  with  $\text{Zr}^{4+}$  by standard synthesis methods [4–6]. The 7.5% Zr/Ti sample treated at 700 °C, prepared in order to attempt a (S)TEM-EDS analysis with a better signal to noise ratio, does not allow the Zr/Ti mapping of the inner crystallite because of the extensive zirconia deposits on the surface, preventing the direct assessment of the diffusion of  $\text{Zr}^{4+}$  in the lattice. Nevertheless, the XRD analysis performed on this sample shows that 67.4% of the total  $\text{Zr}^{4+}$  added into the ink segregates as zirconia. As a consequence, no more than 33% of the added zirconium can diffuse in the lattice (resulting in 2.5% Zr/Ti molar ratio doping). This is highlighted also by the cell parameters measurements (Table 3), where the 7.5% Zr/Ti samples demonstrate cell dimensions comparable with the 1% and 2% Zr/Ti samples instead of the higher values expected in the case of complete zirconium diffusion in the lattice [4].

The BET measurements show a remarkable enhancing effect of the  $\text{Zr}^{4+}$  doping on the specific surface area of the screen-printed titania layers. This is in accordance with the results of the *ex-novo* synthesis of  $\text{Zr}^{4+}$  doped titania reported in literature [4, 6], where the dopant concentration demonstrates a consistent improving effect on the SSA. Our results indicate however, at least for the samples thermally treated at 700 °C, a decrease of the SSA from the 1% to the 2% Zr/Ti layers. This can possibly indicate an uneven diffusion of the Zr on the 2% Zr/Ti samples sintered at  $< 800$  °C and, consequently, that the surface concentration of the  $\text{Zr}^{4+}$  is dependent both on the Zr concentration in the printing ink and on the characteristics of the post deposition thermal treatment. In that case the optimal Zr concentration in the printing ink can be different from the optimal  $\text{Zr}^{4+}$  concentration of an *ex-novo* synthesized titania nanocrystal with a uniform Zr distribution in the crystal lattice.

The in-situ  $\text{Zr}^{4+}$  doping provides greatly support to the photocatalytic activity of the titania layers, stabilizing the anatase phase and thus preventing activity degradation as a consequence of the thermal treatment. Moreover, the activities measured for all screen-printed samples added with  $\text{Zr}^{4+}$  were always higher than those measured for the pure P25 treated at the same temperature, indicating also

a possible catalytic activity enhancement due to the presence of the  $Zr^{4+}$  doping. This is in accordance with several results reported in literature demonstrating that doping with  $Zr^{4+}$  during *ex-novo* synthesis of titania photocatalyst can directly affect the catalytic activity [23–26] by several mechanisms, including the enhanced charge separation in composite  $TiO_2/ZrO_2$  nanocrystals [27], the formation of surface defects on the crystalline structure [4, 28] and the stabilization of the mesoporous structure [7]. This latter is confirmed by the SSA measurements, where the doped samples demonstrate higher SSA values than the undoped ones. The photocatalytic degradation measurements demonstrate also a relative activity decrease from the 1% to the 2% Zr/Ti sample. This can be caused, to some extent, by the relative decrease of the specific surface area measured for the 1% and 2% Zr/Ti samples treated at 700 °C, respectively. The SSA measurements for the 800 °C treated samples indicate however comparable SSA values, suggesting the coexistence of several contributing mechanisms. The increase of the catalytic activity of doped samples can therefore be attributed to the concurrent effects of both the anatase phase stabilization and the  $Zr^{4+}$  doping itself.

## 5. Conclusions

A new and easy scalable approach for the in-situ stabilization of already-formed commercial anatase photocatalysts with  $Zr^{4+}$  organic salt was demonstrated using Degussa P25. The integration of this procedure in the screen-printing process was shown by incorporating a  $Zr^{4+}$  organic salt directly into a screen printing ink.

This new method allows to stabilize the anatase phase for temperature 200 °C higher than the undoped P25 maintaining the same photocatalytic performances. All the doped layers show higher photocatalytic activity for the degradation of toluene than the undoped ones. The activity enhancement can be attributed to both the anatase stabilization and the doping itself.

(S)TEM-EDS analysis of the 2% Zr/Ti molar ratio sample treated at 900 °C demonstrates the zirconium diffusion in the crystal lattice. XRD and TEM analyses demonstrate no evidences of crystalline or amorphous zirconia for the powder samples with Zr/Ti molar ratio  $\leq 2\%$ , suggesting  $Zr^{4+}$  diffusion into titania crystallites also for these ones.

The described in-situ stabilization procedure can be potentially applied to any deposition process involving already-formed anatase photocatalyst, allowing higher sintering temperature and then an improved mechanical stability of the active layers without photocatalytic activity degradation.

## Acknowledgements

This work was supported by ITC-CNR project SP.P04.005, ISTECCNR project ET.P06.010. Dr. M. Marelli gratefully acknowledges the financial support from Regione Lombardia through the project “TIMES, technology and materials for the efficient use of solar energy” – Accordo Quadro Regione Lombardia – CNR. Dr C. Zanelli is gratefully acknowledged for the useful discussion on Rietveld refinement procedure. We thank Mr P. Cardillo for revising the English usage in the manuscript.



## References

- [1] A. Sclafani, J.M. Herrmann, *J. Phys. Chem.* 100 (1996) 13655–13661.
- [2] Dorian A.H. Hanaor, Charles C. Sorrell, *J. Mater. Sci.* 46 (2011) 855–874.
- [3] D.J. Reidy, J.D. Holmes, M.A. Morris, *J. Eur. Ceram. Soc.* 26 (2006) 1527–1534.
- [4] Jimmy C. Yu, Jun Lin, Raymund W.M. Kwok, *J. Phys. Chem. B* 102 (1998) 5094–5098.
- [5] Masanori Hirano, Chiaki Nakahara, Keisuke Ota, Osamu Tanaike, Michio Inagaki, *J. Solid State Chem.* 170 (2003) 39–47.
- [6] N. Venkatachalam, M. Palanichamy, Banumathi Arabindoo, V. Murugesan, *J. Mol. Catal. A-Chem* 266 (2007) 158–165.
- [7] Yu. Gnatyuk, N. Smirnova, O. Kordubanb, A. Eremenkoa, *Surf. Interface Anal.* 42 (2010) 1276–1280.
- [8] K.V. Baiju, C.P. Siby, K. Rajesh, P. Krishna Pillai, P. Mukundan, K.G.K. Warriar, W. Wunderlich, *Mater. Chem. Phys.* 90 (2005) 123–127.
- [9] Jing Liqiang, Sun Xiaojun, Xin Baifu, Wang Baiqi, Cai Weimin, Fu Honggang, *J. Solid State Chem.* 177 (2004) 3375–3382.
- [10] R.Gopalan and Y.S. Lin, *Ind. Eng. Chem. Res.* 34 (1995) 1189–1195.
- [11] Robson F. de Farias, Claudio Airoidi, *J. Non-Cryst. Solids* 351 (2005) 84–88.
- [12] E. Setiawati, K. Kawano, *J. Alloys Comp.* 451 (2008) 293–296.
- [13] E.P. Lokshin, T.A. Sedneva, *Russ. J. Appl. Chem.* 79 (2006) 1238–1241.
- [14] Pradeepan Periyat, Suresh C. Pillai, Declan E. McCormack, John Colreavy, Steven J. Hinder, *J. Phys. Chem. C* 112 (2008) 7644–7652.
- [15] Pradeepan Periyat, Declan E. McCormack, Steven J. Hinder, Suresh C. Pillai, *J. Phys. Chem. C* 113 (2009) 3246–3253.
- [16] Alberto Strini, Alessandra Sanson, Elisa Mercadelli, Alex Sangiorgi, Luca Schiavi, *Thin Solid Films* 545 (2013) 537–542.
- [17] A. Sanson, D. Gardini, G. Montanari, C. Galassi, E. Roncari, *J. Mater. Res.* 21 (2006) 1561–1569.
- [18] S. Gardonio, L. Gregoratti, D. Scaini, C. Castellarin-Cudia, P. Dudin, P. Melpignano, V. Biondo, R. Zamboni, S. Caria, M. Kiskinova, *Organic Electronics* 9 (2008) 253.
- [19] A.C. Larson, R.B.Von Dreele, *General Structure Analysis System (GSAS)*, Los Alamos National Laboratory, Report LAUR 86–748, 2000.
- [20] B.H. Toby, *J. Appl. Cryst.* 34 (2001) 210–213.
- [21] Alberto Strini, Luca Schiavi, *Appl. Catal. B-Environ.* 103 (2011) 226–231.
- [22] R. D. Shannon, *Acta Cryst. A* 32 (1976) 751–767.
- [23] Shengwei Liu, Jiaguo Yu, Stephen Mann, *J. Phys. Chem. C* 113 (2009) 10712–10717.
- [24] Siva Nagi Reddy Inturi, Thirupathi Boningari, Makram Suidan, Panagiotis G. Smirniotis, *Appl. Catal. B-Environ.* 144 (2014) 333–342.
- [25] Lenka Matejová, Kamila Kocí, Martin Reli, Libor Capek, Vlastimil Matejka, Olga Solcová, Lucie Obalová, *Appl. Surf. Sci.* 285P (2013) 688–696.
- [26] J. Choina, Ch. Fischer, G.-U. Flechsig, H. Kosslick, V.A. Tuan, N.D. Tuyen, N.A. Tuyen, A. Schulz, *J. Photochem. Photobiol. A-Chem.* 274 (2014) 108–116.
- [27] Dongfang Zhang, Fanbin Zeng, *Appl. Surf. Sci.* 257 (2010) 867–871.
- [28] Piyawat Supphasrironjaroen, Piyasan Praserttham, Okorn Mekasuwandumrong, Joongjai Panpranot, *Ceram. Int.* 36 (2010) 1439–1446.

Component		Ink 1 no Zr (wt.%)	Ink 2 1% Zr (wt.%)	Ink 3 2% Zr (wt.%)	Ink 4 7.5% Zr (wt.%)
Titania powder (Degussa P25)		27.2	26.7	26.3	24.1
Zr(IV) 2,4-pentanedionate	[17501-44-9]	–	1.6	3.2	11.2
Terpineol	[8000-41-7]	71.1	70.0	68.8	63.2
Lauric acid	[143-07-7]	0.5	0.5	0.5	0.4
Ethyl cellulose	[9004-57-3]	1.2	1.2	1.2	1.1

**Table 1.** Screen-printing ink formulations (weight percentage). Formulation components are identified also by CAS Number. Ink 4 was used only for powder sample preparation.

Sample	Fig. 7	Fig. 8	Ink	Zr/Ti (mol%)	Sintering temp. (°C)	Sintering time (min)	Layer loading (mg cm <sup>-2</sup> )
1	X		1	---	500	30	0.69
2	X		1	---	600	30	0.69
3	X	X	1	---	700	30	0.69
4		X	1	---	700	90	0.72
5		X	1	---	700	180	0.65
6	X		1	---	800	30	0.71
7	X		1	---	900	30	0.65
8	X		1	---	1100	30	0.71
9	X		2	1	500	30	0.75
10	X		2	1	600	30	0.79
11	X	X	2	1	700	30	0.74
12		X	2	1	700	90	0.73
13		X	2	1	700	180	0.79
14	X		2	1	800	30	0.76
15	X		2	1	900	30	0.72
16	X		2	1	1100	30	0.67
17	X		3	2	600	30	0.75
18	X	X	3	2	700	30	0.77
19		X	3	2	700	90	0.77
20		X	3	2	700	180	0.79
21	X		3	2	800	30	0.76
22	X		3	2	900	30	0.74

**Table 2.** Screen-printed samples. The layer loading repeatability is  $\pm 0.01$  mg cm<sup>-2</sup>.

Sample	Anatase cell parameters		
	Zr/Ti	a/b (nm)	c (nm)
0 %	0.37843	0.95059	0.13613
1 %	0.37851	0.95065	0.13620
2 %	0.37854	0.95074	0.13623
7.5 %	0.37853	0.95064	0.13621

**Table 3.** Anatase cell parameters for the powder samples sintered at 700 °C for 30 min.

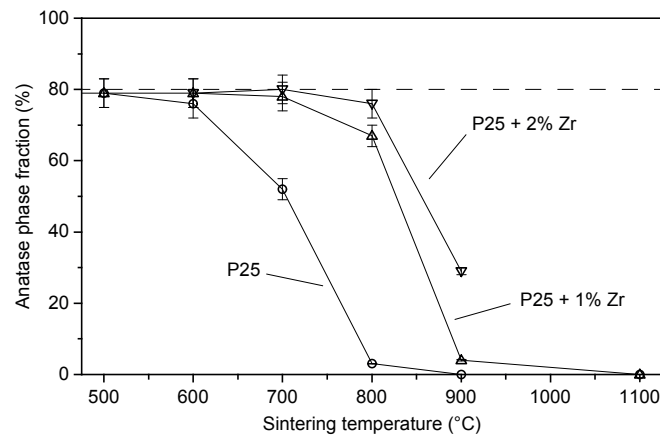


**Figure 1.** Anatase phase fraction (as anatase divided by anatase plus rutile crystalline content) measured with XRD for powder samples with no Zr, 1% Zr/Ti and 2% Zr/Ti molar ratio (1 $\sigma$  error bars). All samples were sintered for 30 min at the indicated temperature. The dashed line indicates the anatase phase fraction of untreated P25.

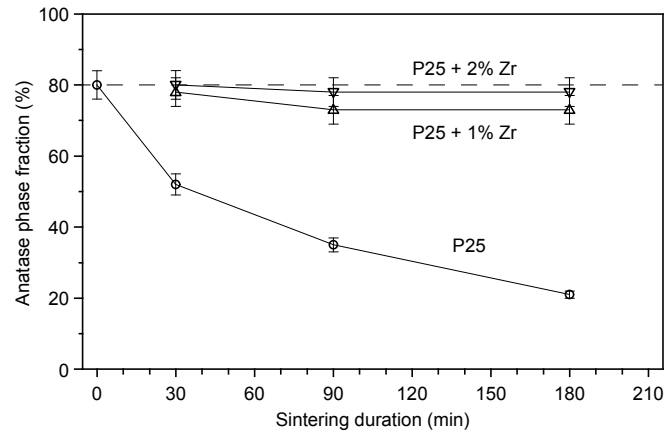


**Figure 2.** Anatase phase fraction (as anatase divided by anatase plus rutile crystalline content) measured with XRD for powder samples with no Zr, 1% Zr/Ti and 2% Zr/Ti molar ratio ( $1\sigma$  error bars). All samples were sintered at 700 °C for the indicated time. The dashed line indicates the anatase phase fraction of untreated P25.

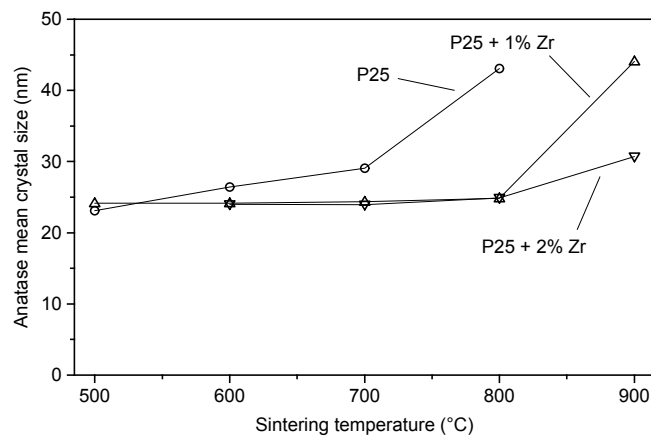


**Figure 3.** Anatase mean crystal size calculated from XRD data for powder samples with no Zr, 1% Zr/Ti and 2% Zr/Ti molar ratio. All samples were sintered for 30 min at the indicated temperature.

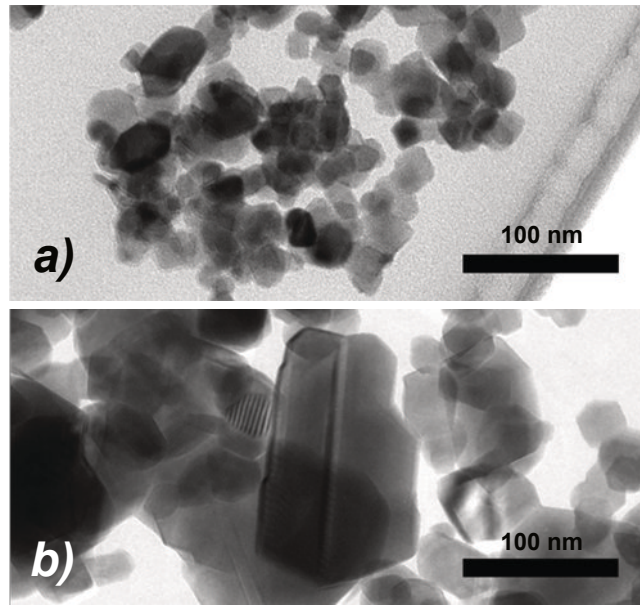


**Figure 4.** TEM images of the 2% Zr/Ti powder samples sintered for 30 min at 500 °C (a) and 900 °C (b), respectively.

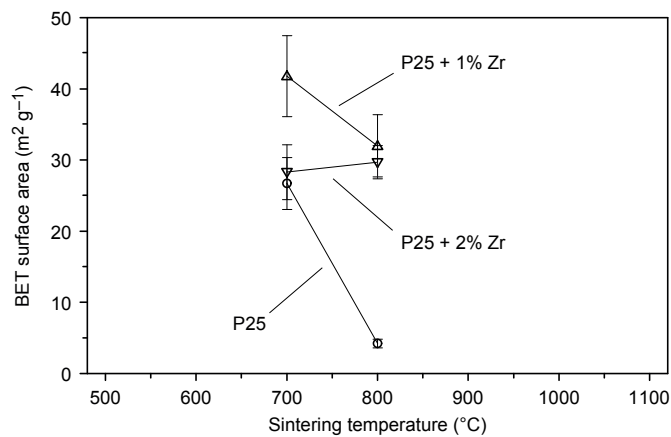


**Figure 5.** Specific surface area of screen-printed samples treated at 700 °C and 800 °C for 30 min. The datum of the 2% Zr/Ti sample treated at 800 °C is the mean of three measurement. Error bars ( $1\sigma$ ) evaluated as described in the text (Section 3.2).



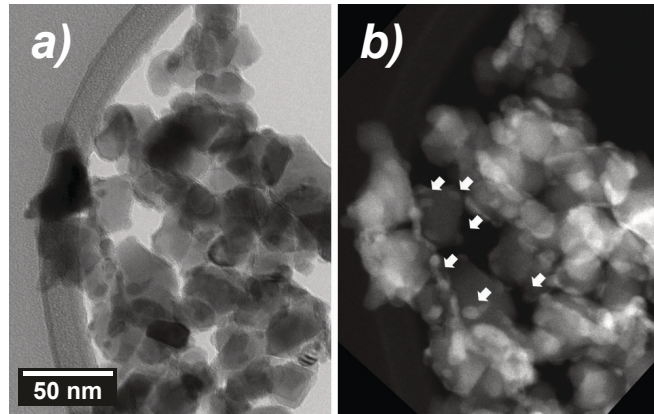


**Figure 6.** TEM (a) and HAADF-STEM (b) images of the same area of the 7.5% Zr/Ti powder sample sintered at 700 °C for 30 min. The arrows indicate some of the zirconia aggregates on the titania crystallite surface.

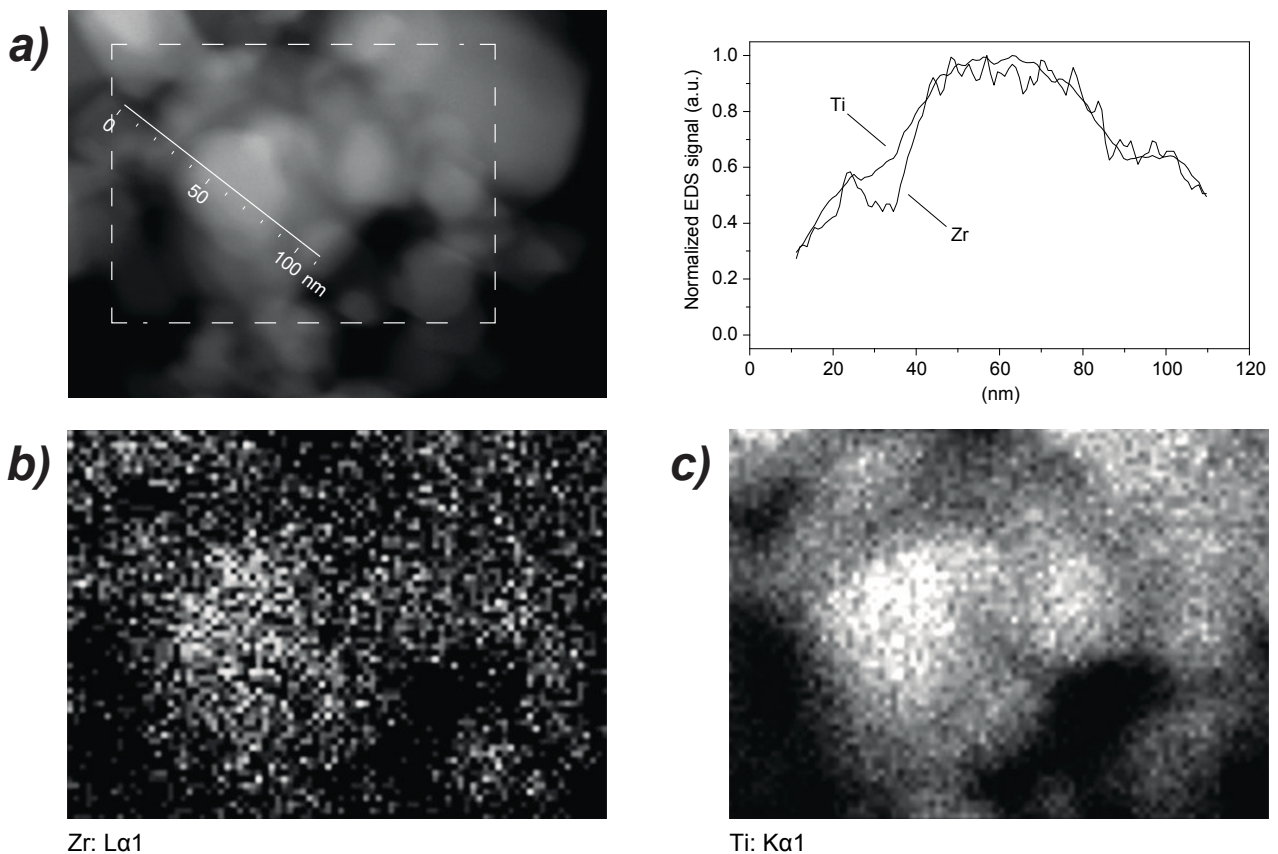


**Figure 7.** STEM-EDS analysis of an anatase crystallite cluster from the 2% Zr/Ti sample sintered at 900 °C for 30 min. Line analysis and related normalized EDS signal profile for zirconium and titanium (a), EDS map for zirconium (b) and titanium (c) for the region of interest marked on (a).

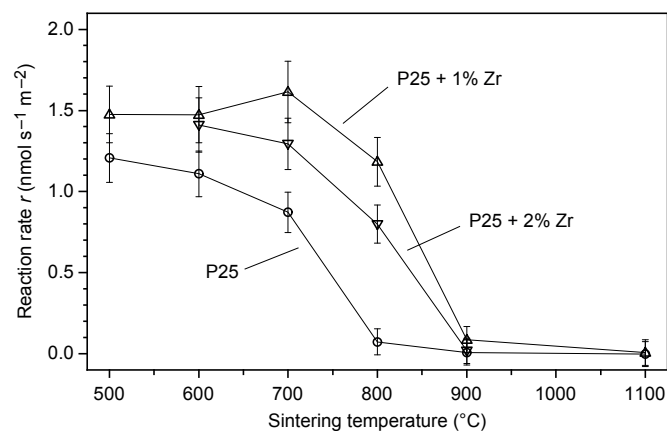


**Figure 8.** Toluene degradation rate  $r$  for screen printed samples with no Zr, 1% Zr/Ti and 2% Zr/Ti molar ratio. All samples were sintered for 30 min at the indicated temperature. Integrated irradiance (340–400 nm)  $182 \pm 5 \mu\text{W cm}^{-2}$ , toluene concentration  $500 \pm 30 \text{ nmol m}^{-3}$ . Error bars ( $1\sigma$ ) computed as described in the text (Section 3.4).

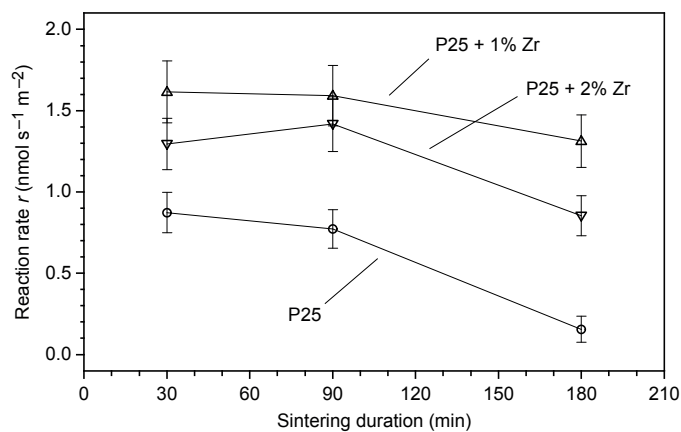


**Figure 9.** Toluene degradation rate  $r$  for screen printed samples with no Zr, 1% Zr/Ti and 2% Zr/Ti molar ratio. All samples were sintered at 700 °C for the indicated times. Integrated irradiance (340–400 nm)  $182 \pm 5 \mu\text{W cm}^{-2}$ , toluene concentration  $500 \pm 30 \text{ nmol m}^{-3}$ . Error bars ( $1\sigma$ ) computed as described in the text (Section 3.4).